Check for updates

Ratiometric fluorescence sensing of temperature based on perovskite nanocrystals and rhodamine B doped electrospun fibers†

Xiaohong Tan,[a] Heng Lu,[a] Yanmei Zhou,[a] Shaoru Wu,[a] Guobin Huang,[c] Xudong Wang,[d] Jingbin Zeng,[e] Feiming Li,[ab] Zhixiong Cai[ab] and Maosheng Zhang [ID] *[ab]

Sensing temperature (T) has gained great attention since T is the most important parameter in daily life, scientific research and industry. A ratiometric fluorescence T sensor is fabricated by doping $MAPbBr_3$ perovskite nanocrystals (PNCs) and rhodamine B (RhB) into a polyacrylonitrile (PAN) matrix and the composite materials are electrospun into optical fibers. The fibers show characteristic emissions at 521 and 587 nm under UV irradiation (λ_{ex} = 365 nm). Both emission intensities gradually increased with elevating T, accompanied with a fluorescence color change from green to yellow. There is a linear relationship between fluorescence intensity ratio (I_{521}/I_{587}) and T in the range of 30–45 °C. The T response sensitivity is as high as 4.38% °C^{-1} at 45 °C.

1. Introduction

Temperature (T) plays a vital role in daily life, scientific research and industry. Constructing a T sensor with high sensitivity, good reliability and real-time response is highly in demand in various fields. Conventional T sensors include resistance T detectors,[1] thermal sensors,[2] infrared T sensors,[3] mercury thermometers and so forth. However, these methods have some limitations, such as expensive equipment and low sensitivity. Fluorescence T sensors have unique properties in that they are able to measure T remotely. The fluorescent materials can be immobilized or painted on the place of interest and signals can be read out via fiber optic technology. Up to now, most fluorescence T sensors were constructed based on a single fluorophore.[4–7] They tend to be strongly influenced by fluorescence background, scattered light, fluctuation of light source and optics. To overcome these problems, ratiometric fluorescence T sensors have been developed.[8–11] Ratiometric sensing of T

utilized two fluorescence emission peaks as signal. Salas-Juárez et al. reported a novel ratiometric fluorescence sensor for monitoring T in the range of 25–100 °C. Lanthanide complex Tb/Eu-TPTZ incorporated in polymethyl methacrylate (PMMA) matrix was used as T-response material.[12] Qiu and coworkers developed a ratiometric T sensor based on the opposite thermal quenching behaviors of Cr^{3+} and Tb^{3+} in a mixture of Cr^{3+}-doped phosphor ($LiAl_5O_8$: Cr^{3+}) and Tb^{3+}-doped phosphor ($LuPO_4$: Tb^{3+}).[13]

Halide perovskites nanocrystals (PNCs) are promising fluorescence materials due to their outstanding characteristics, including high photoluminescence quantum yield (PLQY), narrow emission band, tunable band gap, convenient synthesis and low-cost.[14–18] Methylammonium lead halide perovskites, $MAPbX_3$ (X = Cl, Br, I) PNCs, have attracted increased attention in the fields of solar cells, light-emitting diodes, and photodetectors. However, only few reports on the fluorescence T sensing based on $MAPbX_3$ PNCs, which can be attributed into two reasons: (1) $MAPbX_3$ PNCs are facilitated interference during T sensing due to their poor stability in a humid environment;[19] (2) pure $MAPbX_3$ PNCs have low response sensitivity to T although fluorescence quenching often occurs with increase of T.[20]

Conventionally, encapsulation of halide PNCs into protecting matrices, such as SiO_2,[21] TiO_2,[22] Al_2O_3 (ref. 23) and polymer, are an effective route to enhance their stability. The matrices not only preserve halide PNCs from moisture, oxygen, and UV light, but also reduce the agglomeration of halide PNCs. Electrospinning fibers were used as protecting matrices of halide PNCs, which showed high stability, good surface to volume ratio, increased porosity and high flexibility. Easily accessible polymers, such as PMMA,[24] poly(vinylidene fluoride) (PVDF),[25]

[a]College of Chemistry, Chemical Engineering and Environment, Minnan Normal University, Zhangzhou 363000, China

[b]Fujian Province Key Laboratory of Modern Analytical Science and Separation Technology, Minnan Normal University, Zhangzhou 363000, China

[c]Institute of Food Safety and Environment Monitoring, Fuzhou University, Fuzhou 350108, China

[d]Human Phenome Institute, Fudan University, Shanghai 200438, China

[e]College of Science, China University of Petroleum (East China), Qingdao 266580, China

polyacrylonitrile (PAN)[26] and polystyrene (PS),[27] have been used as electrospinning materials to encapsulate halide PNCs. Surprisingly, encapsulating $MAPbBr_3$ PNCs into PAN electrospinning fibers not only significantly enhance their stability, but also improve their sensitivity to T in the range of 30–45 °C. These properties make them suitable for fluorescence T sensing.

We developed here a novel ratiometric T sensor based $MAPbBr_3$&RhB@PAN fibers by encapsulating $MAPbBr_3$ PNCs and RhB into PAN. The fibers possess two separated fluorescence emission peaks once excited at 360 nm. With the increase of T in the range of 30–45 °C, the fluorescence intensity of $MAPbBr_3$ PNCs increased. Meanwhile, the fluorescence intensity of RhB increased owing to fluorescence resonance energy transfer (FRET). Variation of two fluorescence intensities resulted in fluorescence color change from green to yellow. The proposed ratiometric fluorescence T sensing provided an ingenious method for monitoring T with the advantage of convenience and sensitivity.

2. Results and discussion

2.1. Characterization of PAN, RhB@PAN, $MAPbBr_3$@PAN and $MAPbBr_3$&RhB@PAN fibers

SEM images in Fig. 1a–d show all fibers are long and straight. The surface of PAN and RhB@PAN fibers is rather smooth while the surface of $MAPbBr_3$@PAN and $MAPbBr_3$&RhB@PAN fibers is slightly rough, which may prove the encapsulation of $MAPbBr_3$ PNCs. Furthermore, compared to the diameter of PAN fibers (Fig. 1a, ~1 μm) and RhB@PAN fibers (Fig. 1b, ~1 μm), the diameter of $MAPbBr_3$@PAN fibers (Fig. 1c, ~2.4 μm) and $MAPbBr_3$&RhB@PAN fibers (Fig. 1d, ~3.3 μm) has a significant increase due to the additional $MAPbBr_3$ PNCs. TEM images show that there are abundant nanoparticles (circled in red) dispersed in $MAPbBr_3$@PAN fibers (Fig. 1g) and $MAPbBr_3$&RhB@PAN fibers (Fig. 1h). The lattice fringes with intervals of 0.2 nm are observed in the HRTEM of nanoparticles (the insert image of Fig. 1g) assigned to the d-distance of (242) plane of $MAPbBr_3$ PNCs. Confocal fluorescence microscopy is used to

verify the fluorescence properties of the electrospinning fibers. It is obvious that the PAN fibers exhibit no fluorescence (Fig. 1i). On the contrary, the RhB@PAN fibers (Fig. 1j) and $MAPbBr_3$@PAN fibers (Fig. 1k) show vivid red and green fluorescence, respectively. The $MAPbBr_3$&RhB@PAN fibers (Fig. 1l) display yellow fluorescence which confirms the co-encapsulation of $MAPbBr_3$ PNCs and RhB. In order to verify the $MAPbBr_3$&RhB@PAN fibers are successfully prepared, we measured the elemental composition by EDS, as shown in Fig. S1a–d.† The result indicates the presence of C (25.29%), N (27.05%), O (15.34%), Cl (0.49%), Pb (0.80%) and Br (2.04%) in $MAPbBr_3$&RhB@PAN fibers (Fig. S1d†). By a sharp contrast, pristine PAN fibers (Fig. S1a†) only exist C and N.

The crystal structure of PAN, RhB@PAN, $MAPbBr_3$@PAN and $MAPbBr_3$&RhB@PAN fibers are further characterized by XRD and results are summarized in Fig. 2a. The broad diffraction peak from 15° to 40° of PAN and RhB@PAN fibers indicate they do not have obvious crystal structure. In contrast, the $MAPbBr_3$ (PDF# 76-2758), $MAPbBr_3$@PAN fibers diffraction peaks at 2-theta values are 15°, 21°, 30°, 33.9°, 43° and 45.5° corresponding to (101), (121), (202), (141), (242) and (143) lattice planes, respectively. Peaks at 15° and 30° are assigned to the (101) and (202) of $MAPbBr_3$&RhB@PAN fibers, respectively. It is confirmed that $MAPbBr_3$ PNCs are encapsulated into PAN matrixes by electrospinning fibers. Fig. 2b shows fluorescence spectra of $MAPbBr_3$@PAN, RhB@PAN and $MAPbBr_3$&RhB@PAN fibers. Under the excitation of 360 nm, the $MAPbBr_3$@PAN and RhB@PAN fibers exhibit strong fluorescence emission peaks at 521 with full width at half maximum (FWHM) values of 28 nm and 590 nm with FWHM values of 45 nm, respectively. The fluorescence spectrum of $MAPbBr_3$&RhB@PAN fibers displays dual emission peaks at 521 and 587 nm under the same excitation wavelength which indicates $MAPbBr_3$&RhB@PAN fibers can be used as fluorescence materials of ratiometric fluorescence T sensing. The photographs of the $MAPbBr_3$@PAN, RhB@PAN and $MAPbBr_3$&RhB@PAN fibers under UV light show green, red, and yellow fluorescence, respectively (inset in Fig. 2b). According to these results, the $MAPbBr_3$&RhB@PAN fibers are confirmed to be successfully synthesized.
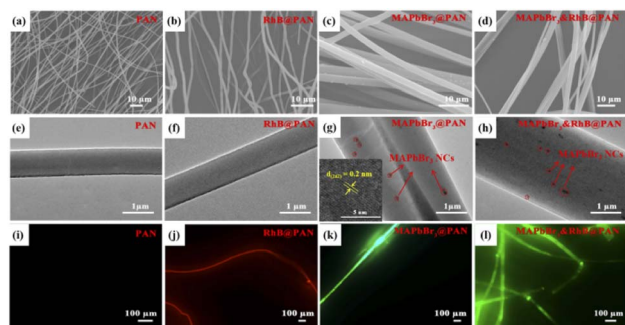

Fig. 1 SEM, TEM and confocal fluorescence microscopic images of the synthesized (a, e and i) PAN fibers, (b, f and j) RhB@PAN fibers, (c, g and k) $MAPbBr_3$@PAN fibers (HRTEM, inset) and (d, h and l) $MAPbBr_3$&RhB@PAN fibers.
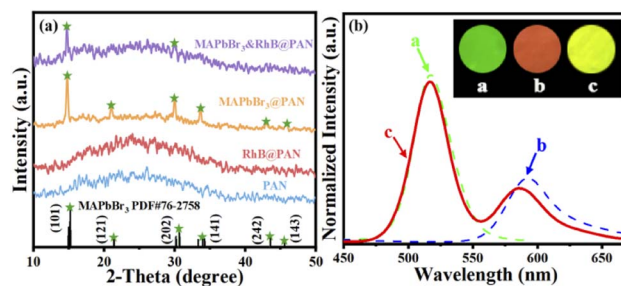

Fig. 2 (a) The XRD patterns of PAN, RhB@PAN, $MAPbBr_3$@PAN and $MAPbBr_3$&RhB@PAN fibers. (b) The fluorescence spectra of the $MAPbBr_3$@PAN fibers (green), RhB@PAN fibers (blue) and $MAPbBr_3$&RhB@PAN fibers (red) (the insert picture of fibers under 365 nm UV illumination).

2.2. Condition optimization for dual-emission ratiometric fluorescence sensing

In order to maximize T sensitivity, several key factors including fluorescence response time and concentration ratio of MAPbBr$_3$ and RhB are studied in details, which has great influence on T sensing response. As shown in Fig. 3, the maximum value of $(I_{521}/I_{587})_0 - (I_{521}/I_{587})$ is observed when MAPbBr$_3$ PNCs and RhB is 9% and 0.1%, respectively. Fig. S2† exhibits that the fluorescence response reaches stable in 10 min after heating in 45 °C. Therefore, 9% MAPbBr$_3$, 0.1% RhB and response time at 10 min are selected as the optimal ratio for the following experiment.

2.3. Stability of MAPbBr$_3$&RhB@PAN fibers

The stability of ratiometric fluorescence T sensor plays a vital role in the field of practical applications. Experiments under different conditions (*i.e.*, ambient air, moisture, and UV-light irradiation) were carried out. As observed in Fig. S3a,† the I_{521}/I_{587} of MAPbBr$_3$&RhB@PAN fibers remain constant during immersing the fibers in water for 15 days. The materials have outstanding hydrophobicity, which is also supported by the fact that the water contact angle of MAPbBr$_3$&RhB@PAN fibers is 116.51° (the insert picture of Fig. S3a†). The I_{521}/I_{587} of MAPbBr$_3$&RhB@PAN fibers nearly remains unchanged for 10 days when storing the material at ambient air (20–25 °C) and relative humidity of 60–80% (Fig. S3b†). The MAPbBr$_3$&RhB@PAN fibers remain stable for at least 4 h under 365 nm UV-light continuous irradiation (Fig. S3c†). Based on these results, it is evident that the hydrophobic PAN can effectively reduce the contact between PNCs and the atmosphere to improve the stability of PNCs.

2.4. Performance of dual-emission ratiometric fluorescence T sensing

The T sensors based on MAPbBr$_3$@PAN and MAPbBr$_3$&RhB@PAN fibers have been constructed under optimized conditions. As shown in Fig. 4a, the fluorescence intensity at 521 nm increases with T increasing, and there is a good linear relationship ($r^2 = 0.9919$) between intensity ratio and T in the range of 30–45 °C (Fig. 4b). The linear regression equation is (Fig. 4b):

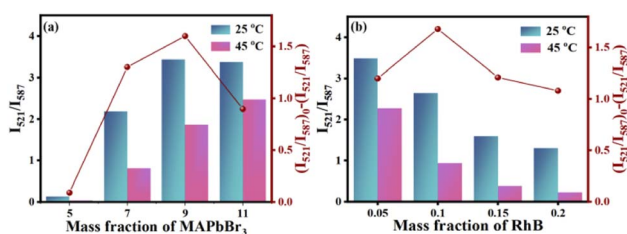$$(I - I_0)/I_0 = 0.702T - 20.603 \tag{1}$$

Fig. 3 Influence of the amounts of (a) MAPbBr$_3$ and (b) RhB at 25 °C and 45 °C of MAPbBr$_3$&RhB@PAN fibers.
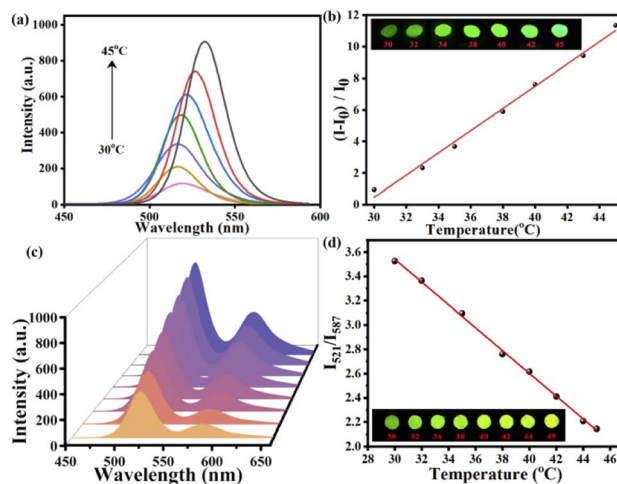
Fig. 4 (a) The fluorescence spectra of the MAPbBr$_3$@PAN fibers in the range of 30–45 °C; (b) linear relationship curve between intensity ratio and T (the insert picture of MAPbBr$_3$@PAN fibers under 365 nm UV illumination). (c) The fluorescence spectra of the MAPbBr$_3$&RhB@PAN fibers in the range of 30–45 °C; (d) linear relationship curve between I_{521}/I_{587} and T (the insert picture of MAPbBr$_3$&RhB@PAN fibers under 365 nm UV illumination).

For MAPbBr$_3$&RhB@PAN fibers, the fluorescence intensity of 521 nm and 587 nm emission peaks all display increase in the range of 30–45 °C (Fig. 4c). Moreover, the calibration plot of I_{521}/I_{587} *versus* T in the range of 30–45 °C displays a good linear with r^2 of 0.9987 (Fig. 4d). The linear curve fit an equation:

$$\Delta = I_{521}/I_{587} = 6.36 - 0.094T \tag{2}$$

The dual emission can be further used for colorimetric sensing of T, in which results can be readout by bare eyes. Obviously, the monochrome color change shown in the insert picture of Fig. 4b is difficult to be distinguished by eyes. However, the MAPbBr$_3$&RhB@PAN fibers show highly distinguishable color change from green to yellow under 365 nm UV-lamp (the insert picture of Fig. 4d).

An important parameter to compare the performance of T sensor is thermal sensitivity, which represents the response of I_{521}/I_{587} with T changing. Absolute sensitivity (S_a) and relative sensitivity (S_r) can be expressed as:[12]

$$S_a = \frac{\partial \Delta}{\partial T} \tag{3}$$

$$S_r = \frac{1}{\Delta} \times \left| \frac{\partial \Delta}{\partial T} \right| \times 100\% \tag{4}$$

From eqn (3), one can see that S_a is the slope in the linear relationship ($S_a = 9.4\%$), which relies on T changing and the material used. S_r can be used to compare the performance of different T sensors (eqn (4)). In our work, S_r value is 4.38% °C^{-1} at the maximum T measured ($T_m = 45$ °C). The Table 1 lists the maximum S_r of different ratio fluorescence T sensing materials

Table 1 Comparison of our work with different materials reports[a]

Materials	T range (°C)	S_r max (% °C^{-1})	Ref.
Zn-TCOMA⊃DMASE	20–60	1.8	10
UiO-66(Zr & Eu)	−36–64	4.26	11
(Tb/Eu-TPTZ)PMMA	25–100	2.98	12
Ad/Tb$_{0.999}$Eu$_{0.001}$/BPDC	−173–27	1.23	30
PP-TzDa	20–100	0.95	31
CsPbBr$_3$@Eu-BTC	20–100	3.9	32
MAPbBr$_3$&RhB@PAN	30–45	4.38	This work

[a] Covalent organic framework (PP-TzDa), 2,4,6-tris(2-pyridyl)-1,3,5-triazine (TPTZ), Zn-based metal–organic framework (Zn-TCOMA), 4-(4-(dimethylamino)styryl)-1-ethylpyridinium (DMASE), biphenyl-4,4′-dicarboxylate (BPDC), adeninate (Ad).

in different T ranges. Compared with other materials, MAPbBr$_3$&RhB@PAN fibers have a higher S_r value at lower T. And the morphological of MAPbBr$_3$&RhB@PAN fibers shows negligible change in different T (Fig. S4†). The thermal stability of MAPbBr$_3$&RhB@PAN fibers is evaluated by TGA curves, which can be roughly divided into three weight loss stages as shown in Fig. S5†.[28,29] The fibers lose about 8% of the initial weight from 30 °C to 287 °C in the first stage, which is mainly attributed to evaporation of water molecules on the surface of fibers and low boiling temperature volatile compounds (DMF). In the range from 287 to 460 °C, there is a sudden decline (weight loss is about 45%), signifying a cyclization, dehydrogenation and thermal cross-linking process of PAN. In the third stage above 460 °C, the weight loss takes place at a relatively steady pace as for MAPbBr$_3$&RhB@PAN fibers, which might be resulted from the partial evaporation of NH$_3$ and HCN. From the analysis above, the novel ratiometric fluorescence T sensor could be constructed by MAPbBr$_3$&RhB@PAN fibers, which indicates that the ratiometric fluorescence T sensor had a potential application for on-site T measurement.

2.5. Mechanism of ratiometric fluorescence T sensor MAPbBr$_3$&RhB@PAN fibers

Generally, the fluorescence intensity of fluorescence materials decreases with increasing T due to thermal quenching. However, MAPbBr$_3$@PAN fibers show reverse trends, whose intensity increases markedly with increasing T in the range of 30–45 °C. According to literature, the fluorescence enhancement with increasing T may be attributed to the followed reasons: (1) the aggregation degree of PNCs is lower at higher T and results in decreased concentration quenching of fluorescence. However, this phenomenon often occurs in solution system, not in polymer fibers;[33] (2) delayed fluorescence can lead to the increase of fluorescence intensity with increasing T, when the fluorescence lifetime of fluorescence materials is about several milliseconds.[34,35] However, in our case, the fluorescence lifetime of MAPbBr$_3$@PAN fibers is about several nanoseconds; (3) the thermally activated passivation can also enhance by reducing the surface defects of PNCs, thus resulting in fluorescence enhancement with increasing T. For MAPbBr$_3$@PAN fibers, the nitrile grouping (–CN) in PAN can passivate MAPbBr$_3$ PNCs since it is easy to form strong
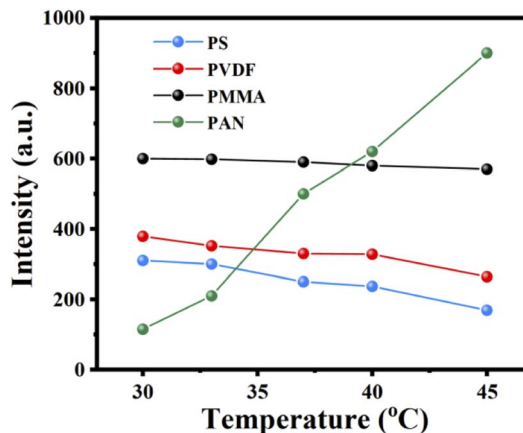

Fig. 5 The fluorescence intensity of the MAPbBr$_3$@PS (blue), MAPbBr$_3$@PVDF (red), MAPbBr$_3$@PMMA (black) and MAPbBr$_3$@PAN (green) fibers in the range of 30–45 °C.

coordination bonds with Pb^{2+} after thermal treatment. This result is similar to Xie's report.[36] As further proof, MAPbBr$_3$@PS, MAPbBr$_3$@PVDF and MAPbBr$_3$@PMMA fibers are synthesized and their T sensitive experiment are investigated. As shown in Fig. 5, except MAPbBr$_3$@PAN fibers, fluorescence intensity of other fibers decrease with increasing T. The fluorescence spectra of RhB@PAN fibers are shown in Fig. S6.† The fluorescence intensity of RhB in RhB@PAN fibers shows negligible change after thermal treatment under 360 nm excitation (Fig. S6a†). Surprisingly, the fluorescence intensity of RhB increases with increasing T in MAPbBr$_3$&RhB@PAN fibers (Fig. S6b†). We believe this result is directly related to the FRET from MAPbBr$_3$ PNCs to RhB in MAPbBr$_3$&RhB@PAN fibers.[37]

FRET is the process of nonradiative energy transfer between fluorescent donor and light-absorbing receptor. The occurrence of FRET highly depends on the extent of spectral overlap and the distance between the donor and receptor. FRET rate can be calculated to related parameters such as Förster distance (R_0), overlap integral ($J(\lambda)$) and energy transfer efficiency (E). It can be found in Fig. S7a,† the absorbance spectrum of RhB significantly overlaps the emission spectrum of MAPbBr$_3$ PNCs. R_0 should be between the range of approximately 1 to 10 nm of donor and receptor in FRET, defined as follows:[38]

$$R_0 = 8.8 \times 10^{-25} K^2 n^{-4} \psi J(\lambda) \tag{5}$$

where K^2 is orientation factor (the random orientation factor in space is 0.476), n is refractive index of the medium (PAN is 1.514), ψ is quantum efficiency of the donor and $J(\lambda)$ is overlap integral between fluorescence emission spectrum of the energy donor and absorption spectrum of the energy receptor, which can be calculated by the following eqn (6):[38]

$$J(\lambda) = \int_0^\infty F_D(\lambda)\varepsilon_A(\lambda)\lambda^4 d\lambda \tag{6}$$

where $F_D(\lambda)$ is the fluorescence spectrum of the donor and $\varepsilon_A(\lambda)$ is the molar extinction coefficient of the receptor at wavelength λ. The R_0 of MAPbBr$_3$ and RhB can be calculated as 9.07 nm,

which conforms to Förster distance of FRET theory between 1 and 10 nm. The value of E is estimated to be 52.6%, according to eqn (7):[38]

$$E = 1 - \frac{I_{DA}}{I_A} \qquad (7)$$

where I_{DA} and I_A are, respectively, the MAPbBr$_3$ PNCs (donor) fluorescence intensity at 360 nm with and without the presence of RhB (receptor).

Thus, the proposed FRET mechanism is depicted in Fig. S7b.† Under 365 nm UV light, MAPbBr$_3$ PNCs absorb photons and then are excited to a higher electronic energy state (excited state). MAPbBr$_3$ PNCs in the excited state return to the ground state after transferring the energy to the RhB through the dipole interaction between MAPbBr$_3$ PNCs and RhB, which cause the intensity of RhB increase.

3. Conclusions

In summary, a novel ratiometric fluorescence T sensor has successfully been constructed by doping MAPbBr$_3$ PNCs and RhB into PAN fibers *via* electrospinning technique. The amounts of MAPbBr$_3$ PNCs and RhB was optimized to improve T sensing sensitivity. When the T rising, both fluorescence intensities of MAPbBr$_3$ and RhB increase due to passivation and FRET, respectively. There is apparent fluorescence color change with increasing T which can be inspected by bare eyes under 365 nm UV-lamp. There is a good linear relationship between fluorescence ratio and T in the range of 30–45 °C. The MAPbBr$_3$&RhB@PAN fibers exhibit excellent performance with a high relative sensitivity of 4.38% °C^{-1}. The colorimetric sensor provides a new method for on-site T measurement for its convenient synthesis and low-cost, which indicates the application prospect in T sensing.

Conflicts of interest

The authors declared that they have no conflicts of interest to this work.

Acknowledgements

Notes and references

1 L. Okte, A. Raman, B. Raj and N. Kumar, *Silicon*, 2021, 1–11.
2 P. Jin, L. Xu, T. Jiang, L. Zhang and J. Huang, *Int. J. Heat Mass Transfer*, 2020, **163**, 120437–120446.
3 H. Y. Chen, A. Chen and C. Chen, *Sensors*, 2020, **20**, 2885–2902.
4 B. Li, *J. Coord. Chem.*, 2020, **73**, 429–438.
5 S. Wang, J. Cao and C. Lu, *New J. Chem.*, 2020, **44**, 4547–4553.
6 A. Vysniauskas, B. Cornell, P. S. Sherin, K. Maleckaite, M. Kubankova, M. A. Izquierdo, T. T. Vu, Y. A. Volkova, E. M. Budynina, C. Molteni and M. K. Kuimova, *ACS Sens.*, 2021, **6**, 2158–2167.
7 Y. Sun, W. He, X. Sun and B. Liu, *Luminescence*, 2020, **35**, 1416–1423.
8 Y. Yang, L. Lin, P. Lu, Z. Feng, Z. Li, J. Cai, Z. Mei, Y. Huang, W. Guo, Z. Wang and Z. Zheng, *J. Lumin.*, 2021, **240**, 118410–118418.
9 X. Sun, L. Cai, W. He, X. Cao, B. Liu and H. Wang, *Spectrochim. Acta, Part A*, 2022, **264**, 120266–120274.
10 Y. Wan, Y. Cui, Y. Yang and G. Qian, *Chin. Chem. Lett.*, 2021, **32**, 1511–1514.
11 J. F. Feng, T. F. Liu, J. Shi, S. Y. Gao and R. Cao, *ACS Appl. Mater. Interfaces*, 2018, **10**, 20854–20861.
12 C. J. Salas-Juárez, R. E. Navarro, A. Pérez-Rodríguez, U. Orozco-Valencia and R. Aceves, *Sens. Actuators, A*, 2020, **315**, 112293.
13 L. Qiu, P. Wang, X. Wei, F. Chi, Y. Chen and M. Yin, *J. Alloys Compd.*, 2021, **879**, 160461.
14 H. Si, C. Xu, G. Ou, G. Zhang, W. Fan, Z. Xiong, A. Kausar, Q. Liao, Z. Zhang, A. Sattar, Z. Kang and Y. Zhang, *Nano Energy*, 2020, **68**, 104320.
15 Y. Yang, D. Wu, Z. Zhang, W. Cao, X. Zhao, Y. Hao, P. Yang and J. Wang, *Chem. Phys. Lett.*, 2020, **759**, 137985–137991.
16 X. Min, Q. Xie, X. Wang and M. Chen, *Surf. Interfaces*, 2021, **22**, 100870–100884.
17 L. Protesescu, S. Yakunin, M. I. Bodnarchuk, F. Krieg, R. Caputo, C. H. Hendon, R. X. Yang, A. Walsh and M. V. Kovalenko, *Nano Lett.*, 2015, **15**, 3692–3696.
18 Y. Zhao, J. Li, Y. Dong and J. Song, *Isr. J. Chem.*, 2019, **59**, 649–660.
19 Z. Liu, Y. Zhang, Y. Fan, Z. Chen, Z. Tang, J. Zhao, Y. Lv, J. Lin, X. Guo, J. Zhang and X. Liu, *Surf. Interfaces*, 2018, **10**, 13053–13061.
20 A. Dualeh, P. Gao, S. I. Seok, M. K. Nazeeruddin and M. Grätzel, *Chem. Mater.*, 2014, **26**, 6160–6164.
21 Q. Zhong, M. Cao, H. Hu, D. Yang, M. Chen, P. Li, L. Wu and Q. Zhang, *ACS Nano*, 2018, **12**, 8579–8587.
22 Z. J. Li, E. Hofman, J. Li, A. H. Davis, C. H. Tung, L. Z. Wu and W. Zheng, *Adv. Funct. Mater.*, 2017, **28**, 1704288.
23 G. Longo, A. Pertegás, L. Martínez-Sarti, M. Sessolo and H. J. Bolink, *J. Mater. Chem. C*, 2015, **3**, 11286–11289.
24 G. Jiang, C. Guhrenz, A. Kirch, L. Sonntag, C. Bauer, X. Fan, J. Wang, S. Reineke, N. Gaponik and A. Eychmuller, *ACS Nano*, 2019, **13**, 10386–10396.
25 G. Huang, Y. Zhou, F. Li, X. Tan, Z. Cai, D. Luo, T. Chen and M. Zhang, *Sens. Actuators, B*, 2021, **347**, 130618.
26 J. Lu, L. Zhang, C. Peng, L. Rao and M. Wan, *Chem. Lett.*, 2016, **45**, 312–314.
27 X. Liang, M. Chen, Q. Wang, S. Guo and H. Yang, *Angew. Chem., Int. Ed. Engl.*, 2019, **58**, 2799–2803.
28 X. Zhang, Y. Qi, J. Yang, S. Dong, J. Liu, J. Li and K. Shi, *Polym. Degrad. Stab.*, 2021, **191**, 109680.
29 Q. Niu, Q. Zhu, Y. Tang, J. Nie and G. Ma, *Mater. Sci. Eng., C*, 2017, **77**, 326–332.

30 X. Shen, Y. Lu and B. Yan, *Eur. J. Inorg. Chem.*, 2015, **2015**, 916–919.

31 M. Huang, J. Chong, C. Hu and Y. Yang, *Inorg. Chem. Commun.*, 2020, **119**, 108094–108099.

32 J. Liu, Y. Zhao, X. Li, J. Wu, Y. Han, X. Zhang and Y. Xu, *Cryst. Growth Des.*, 2019, **20**, 454–459.

33 L. N. Sun, J. Yu, H. Peng, J. Z. Zhang, L. Y. Shi and O. S. Wolfbeis, *J. Phys. Chem. C*, 2010, **114**, 12642–12648.

34 A. G. Joly, W. Chen, J. Roark and J. Z. Zhang, *J. Nanosci. Nanotechnol.*, 2001, **1**, 295–301.

35 M. Engeser, L. Fabbrizzi, M. Licchelli and D. Sacchi, *Chem. Commun.*, 1999, **18**, 1191–1192.

36 J. Xie, K. Yan, H. Zhu, G. Li, H. Wang, H. Zhu, P. Hang, S. Zhao, W. Guo, D. Ye, L. Shao, X. Guan, T. Ngai, X. Yu and J. Xu, *Sci. Bull.*, 2020, **65**, 1726–1734.

37 Y. Wang, Y. Zhu, J. Huang, J. Cai, J. Zhu, X. Yang, J. Shen, H. Jiang and C. Li, *J. Phys. Chem. Lett.*, 2016, **7**, 4253–4258.

38 M. Cardoso Dos Santos, W. R. Algar, I. L. Medintz and N. Hildebrandt, *TrAC, Trends Anal. Chem.*, 2020, **125**, 115819.